Applied Catalysis A, General 606 (2020) 117809

Contents lists available at ScienceDirect

Applied Catalysis A, General

journal homepage: www.elsevier.com/locate/apcata

Enhancing electrochemical nitrate reduction toward dinitrogen selectivity on Sn-Pd bimetallic electrodes by surface structure design

Jenn Fang Su[a,b], Wei-Fan Kuan[c], Ching-Lung Chen[a,d,e], Chin-Pao Huang[a,*]

[a] Department of Civil and Environmental Engineering, University of Delaware, Newark, DE 19716, USA
[b] Department of Chemical and Materials Engineering, Tamkang University, New Taipei City, 25137, Taiwan
[c] Advanced Materials Characterization Laboratory, University of Delaware, Newark, DE, 19716, USA
[d] Department of Safety, Health and Environmental Engineering, Ming Chi University of Technology, New Taipei City, 24301, Taiwan
[e] Center for Environmental Sustainability and Human Health, Ming Chi University of Technology, New Taipei City, 24301, Taiwan

ARTICLE INFO

Keywords:
Sn-Pd bimetallic electrode
Nitrate reduction
Dinitrogen selectivity
Surface structure

ABSTRACT

Bimetallic palladium (Pd) and tin (Sn) catalysts were electrochemically deposited on stainless steel mesh support by controlling the metal deposition sequence, total electrical charge, and metal composition. Results showed that the preparation procedure affected the crystal structure of bimetallic Pd-Sn catalysts, which significantly influenced nitrate removal efficiency and dinitrogen selectivity. Electrode with Sn on the outside surface exhibited relatively greater nitrate removal rate constant and nitrate conversion. The Sn to Pd molar ratio and the electrical charge applied during electrode preparation also affected the nitrate reduction performance. The SS/$Sn_{0.2}Pd_{0.8}$-497 electrode exhibited 88, 89, 79, and 9% of total nitrate removal, dinitrogen selectivity, dinitrogen yield, and NH_4^+ selectivity, respectively. Among the three major facets, (214), (131) and (420) of Sn_3Pd alloy on the electrode surface, (420) exhibited the most critical effect on the dinitrogen yield. Crystal structure of catalysts controls the reactivity and selectivity of electrochemical reduction as exemplified by nitrate.

1. Introduction

Nitrate is a major groundwater contaminant in the United States and world. According to US Geological Survey (USGS), about 7% of 2400 private wells show nitrate concentration exceeding the U. S. Environmental Protection Agency (USEPA) drinking water standard of 10 mg/L. Natural nitrate level in groundwater is typically lower than 10 mg/L. Excessive nitrate concentration is mainly caused by anthropogenic sources, inefficient use of fertilizers, improper disposal of nitrate-laden domestic sewage, agricultural or industrial wastewater, and emissions from combustion engines. High nitrate level in drinking water may cause methemoglobinemia in infants and gastrointestinal cancer in adults, therefore there is urgent need of efficient and sustainable technology for the renovation of nitrate-contaminated water is ever-growing.

Common physical-chemical methods for nitrate removal include adsorption (e.g., ion exchange resins) [1], concentration, e.g., reverse osmosis [2] and electrodialysis [3]. These methods are reliable, effective, fast, easy to operate, and appealing to both small and medium-size water and wastewater treatment plants [4,5]. However, the above methods do not transform nitrate to benign species, specifically nitrogen gas.

As far as drinking water purification is concerned, chemical reduction process [6–10] has numeral advantages over above physical-chemical methods, such as fast reaction, easy operation, and generation of relatively benign nitrogen by-products. Unfortunately, ammonia is an inevitable byproduct in most chemical reduction processes. Post-treatment processes for ammonium ion removal, such as ion exchange resins or gas stripping are always needed as to safeguard drinking water safety, thereby requiring additional treatment costs.

Electrochemical method is a green approach for the water/wastewater treatment industry [11–16]. It offers a number of advantages over traditional treatment processes such as environmental compatibility, safety, energy efficiency, selectivity, and versatility.Additionally, electrochemical processes do not generally produce secondary pollutants, therefore, reduce process significant treatment costs relative to biodegradation and conventional chemical treatment methods.

A wide variety of cathodic metals and alloys including Pt [17], Pd [18], Cu [19], Ag [20], Rh [21], Sn [22], Pb [23], Cu-Pt [24], Cu-Sn [25], Cu-Zn [26], Cu-Pb [20], Cu-Fe [27], Cu-Ni [20,28], Cu-Pd [29–32], and Sn-Pd [29,33,34] have been studied for electrochemical nitrate reduction. Recently, many studies have focused on

---

[*] Corresponding author.
E-mail address: huang@udel.edu (C.-P. Huang).

https://doi.org/10.1016/j.apcata.2020.117809
Received 26 June 2020; Received in revised form 26 August 2020; Accepted 27 August 2020

Table 1
Synthetic detail of bimetallic electrodes.

Samples	First loading							Second loading							Q^a	Pd/Sn metal ratio
	Metal	Current (A)	Time (sec)	Cycles	Current (A)	Time (sec)	Cycles	Metal	Current (A)	Time (sec)	Cycles	Current (A)	Time (sec)	Cycles		
$SS/Pd_{0.2}Sn_{0.8}$-497	Pd	0.3	30	6	0.6	90	1	Sn	0.3	108	6	0.6	324	1	497	1/4
$SS/Sn_{0.8}Pd_{0.2}$-497	Sn	0.3	108	6	0.6	324	1	Pd	0.3	30	6	0.6	90	1	497	1/4
$SS/Sn_{0.8}Pd_{0.2}$-166	Sn	0.3	36	6	0.6	108	1	Pd	0.3	10.2	6	0.6	30	1	166	1/4
$SS/Sn_{0.8}Pd_{0.2}$-332	Sn	0.3	72	6	0.6	216	1	Pd	0.3	20.4	6	0.6	60	1	332	1/4
$SS/Sn_{0.8}Pd_{0.2}$-1490	Sn	0.3	324	6	0.6	972	1	Pd	0.3	90	6	0.6	270	1	1490	1/4
$SS/Sn_{0.5}Pd_{0.5}$-497	Sn	0.3	69	6	0.6	207	1	Pd	0.3	69	6	0.6	207	1	497	1
$SS/Sn_{0.2}Pd_{0.8}$-497	Sn	0.3	30	6	0.6	90	1	Pd	0.3	108	6	0.6	324	1	497	4

[a] Q is the total charge (C = I x t), I is current (A), and t is the deposition time (sec).

electrochemical denitrification using bimetallic systems as the addition of a second metal seemed to significantly has improved the nitrate reactivity, nitrogen selectivity, and electrode stability. Bandarenka and Koper [35], studied the electrochemical reduction of nitrate using various monolayer/substrate electrocatalysts and reported that the presence of a second metal (monolayer) on the electrode surface selectively produced preferential products, such as NO (on Cu/Pt), N_2O (on Sn/Pt), NH_2OH (on Ge/Pd), or $NH_4{}^+$ (on Sn/Pd) [35]. Roué et al. studied the conversion of nitrate to nitrogen over monometallic Cu [36,37] and bimetallic $Cu_{0.7}Ni_{0.3}$ electrode [37], and reported that nitrate conversion over the $Cu_{0.7}Ni_{0.3}$ bimetallic electrode (92%) was about two times that on the Cu electrode (49%) [36,37]. Xu et al. demonstrated that $Cu_{0.8}Ni_{0.2}$ and $Cu_{0.8}Pb_{0.2}$ bimetallic electrodes exhibited decreasing ammonia selectivity while improving nitrogen yield compared to Cu monometallic electrode [38]. Although theoretical and experimental studies have demonstrated the superiority of bimetallic catalysts in electrochemical nitrate reduction, a direct 100% selectivity of nitrate reduction to nitrogen gas remains the ultimate goal and challenge. Therefore, there were increasing interests on the development of new electro-catalytic materials with improved N_2 selectivity in the last few years.

Koper et al. studied the electrochemical activity for nitrate reduction using density function theory (DFT) calculations incorporated with a series of laboratory experiments and demonstrated that electrochemical nitrate reduction was electrode structure sensitive and that a perfect monometallic and monocrystalline Pt(100) crystal phase yielded the highest catalytic activity [39–43]. Most significantly, Koper et al. reported that active sites consisting of a square or rectangular arrangement involving four surface metallic atoms on the Pt(100) phase were essential to most bond-breaking reactions because of higher bonding energy between bond-breaking precursors and electrode surface atoms [44]. On the contrary, the appearance of Pt(111) phase, atoms arranged in diamond shapes, would lead to a decrease in catalytic activity because of weak binding energy [35]. Kato et al. compared the catalytic activity of tin-modified single crystalline electrodes of palladium, platinum and palladium-platinum alloy with the (111) surface versus the (100) surface on nitrate reduction and concluded that the tin-modified (100) surface exhibited greater nitrate reactivity than that of the (111) surface in acid and neutral media [45].

In short, it has been reported recently reported that the reactivity and selectivity of nitrate reduction in water was significantly influenced by the surface roughness and crystallite size of bimetallic electrodes [34]. The general reaction mechanism was proposed as the following:

$$NO_3^- + Sn \rightleftarrows Sn[NO_3^-] \tag{1a}$$

$$H^+ + Pd + e^- \rightleftarrows Pd[H] \tag{1b}$$

$$Sn[NO_3{}^-] + 2\,Pd[H] \rightarrow Sn[NO_2{}^-] + Pd[H_2O] \tag{1c}$$

$$Sn[NO_2{}^-] + Pd[H] \rightarrow Sn[NO] + Pd[OH^-] \tag{1d}$$

$$2\,Sn[NO] + 2\,Pd[H] \rightarrow Sn[N_2O] + Pd[H_2O] + Sn + Pd \tag{1e}$$

$$Sn[N_2O] + 2\,Pd[H] \rightarrow Sn[N_2] + Pd[H_2O]\ (1f) \rightarrow Sn[N_2] + Pd[H_2O] \tag{1f}$$

$$Sn[N_2] \rightarrow Sn + N_2 \tag{1g}$$

$$Sn[NO] + Pd[H] \rightarrow Pd[NH] + Sn[O] \tag{1h}$$

$$Pd[NH] + Pd[H] \rightarrow Pd[NH_2] + Pd \tag{1i}$$

$$Pd[NH_2] + Pd[H] \rightarrow Pd[NH_3] + Pd \tag{1j}$$

$$Pd[NH_3] \rightarrow NH_3 + Pd \tag{1k}$$

$$NH_3 + H_2\,O \rightleftarrows NH_4^+ + OH^- \tag{1l}$$

The major reaction scheme included: (i) adsorption of nitrate onto

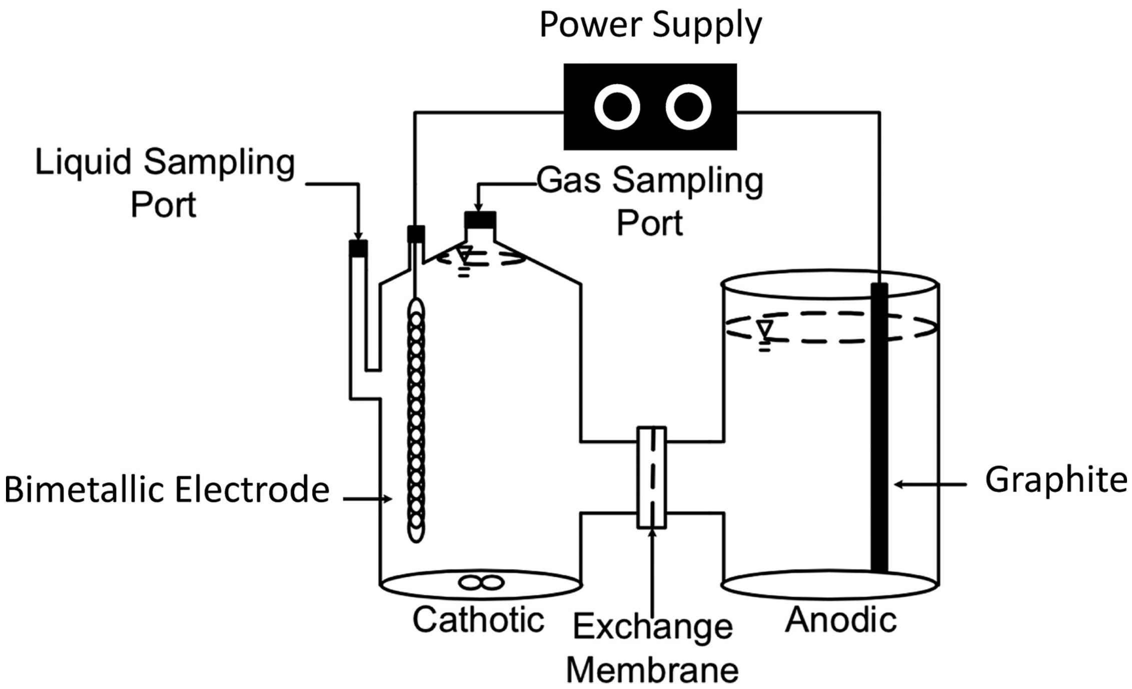

Fig. 1. Schematic diagram of electrochemical nitrate reduction experiments.

an empty Sn site via its oxygen atoms; (ii) adsorption of hydrogen on the empty Pd site; (iii) direct surface electrochemical reduction of nitrate to nitrite; (iv) a series of surface reactions involving the surface hydrogen atoms (on the Pd site) and various surface oxy-nitrogen species (on the Sn site), which eventually led to the formation of nitrogen molecules; (v) further reaction between the surface hydrogen species and surface oxy-nitrogen species generated ammonium ion.

The present study was our continuing effort to further explore the effects of catalyst preparation process on the electrode surface structure and how such alloy surface structure affected the reactivity and selectivity of nitrate reduction. Most previous work in bimetallic electrodes studied and discussed the influence of bimetal ratio on the selectivity of the nitrate reduction pathway [46–50]. To the best of our knowledge, this is among the first study to investigate the surface structure design and surface atom arrangements of bimetallic alloy electrodes and its correlation to nitrate reduction performance and selectivity. In the present study, we modified the metal deposition sequence, the total electrical charge applied, and the atomic ratio between the two metals as a means to control the surface property of the bimetallic electrode. It was hypothesized that adjusting the crystal facets on electrode surface would influence the bond-breaking and bond-formation reactions among nitrate ions, electrode surface, and reaction intermediates, thereby enhancing nitrate reactivity and nitrogen selectivity. Tin-modified palladium, Sn-Pd, catalyst was selected for this study, in which Sn was intended to be the O-affinity and Pd be the H-adsorbing metal, respectively, due to its high reactivity compared to Cu-Pd [33,51]. This work aimed at developing a synthesis procedure for better design of specific electrochemical electrodes of high efficiency in transforming nitrate to benign nitrogen gas for water treatment applications.

2. Materials and methods

2.1. Materials

Sodium nitrate was obtained from Fisher Scientific, Pittsburgh, PA, USA (ACS certified grade). Perchloric acid was purchased from ACROS, Fair Lawn, NJ, USA. Sodium hydroxide (purity > 97.0%) and methanesulfonic acid were purchased from Sigma-Aldrich, St Luis, MO USA. Deionized water was treated with Mega-Pure System (Model MP-290). Platinum wire (Fisher Scientific, 1284987, od: 0.5 mm) was purchased from Fisher Scientific, Pittsburgh, PA, USA. Stainless steel mesh (corrosion-resistant 304 stainless steel woven wire cloth, 100 × 100 mesh, 0.0045″ wire diameter) was obtained from McMaster-Carr Co. Elmhurst, IL USA. For catalytic material preparation, tin (II) chloride (purity > 98%), and palladium (II) chloride (purity > 98%) were purchased from Sigma-Aldrich, St Luis, MO USA. All chemicals were used as received without further purification.

2.2. Electrode preparation

The electrode preparation procedure was as follows. The raw stainless-steel mesh (SS) was cut into small pieces (ca. 1.5 cm × 8 cm) and washed with detergent thoroughly. Afterward, the SS mesh was rinsed with deionized water several times then dried in a dryer at room temperature for 1 h. The metal ion solutions were prepared by dissolving tin chloride ($SnCl_2$) and palladium chloride ($PdCl_2$) in deionized water at concentration of 0.1 M and 0.01 M, respectively. All electrodeposition experiments were carried out at room temperature by using a two-electrode system, which was connected to a potentiostat (Model WP705B, Vector-VID). Graphite (ca. 1.5 cm × 8 cm) was the anode and the surface-cleaned SS was the cathode. Both electrodes were immersed in the metal ion solution in a 250-mL beaker. Metal deposition process was performed first at the constant current of 0.3 A @1.8 min for 6 times (total 10.8 min), and then increased current to 0.6 A for 1 min for additional deposition of both metals, with Sn being deposited ahead of Pd. For example, a typical SS/Sn-Pd electrode was prepared by immersing the SS in the 0.1 M $SnCl_2$ solution for Sn deposition at 0.3 A @ 1.8 min for 6 repeating times (total 10.8 min), and then the current was increased to 0.6 A to continue deposit Sn for another 5.4 min to complete prepare the SS/Sn precursor electrode. This multi-step electrodeposition was necessary for better nitrate reduction performance as detailed previously [34]. The SS/Sn precursor electrode was rinsed with deionized water followed by immersing in 0.01 M $PdCl_2$ solution for Pd deposition at 0.3 A for 6 times @ 0.5 min followed by continuous deposition at 0.6 A for 1 time @1.5 min. Finally, the electrode was washed

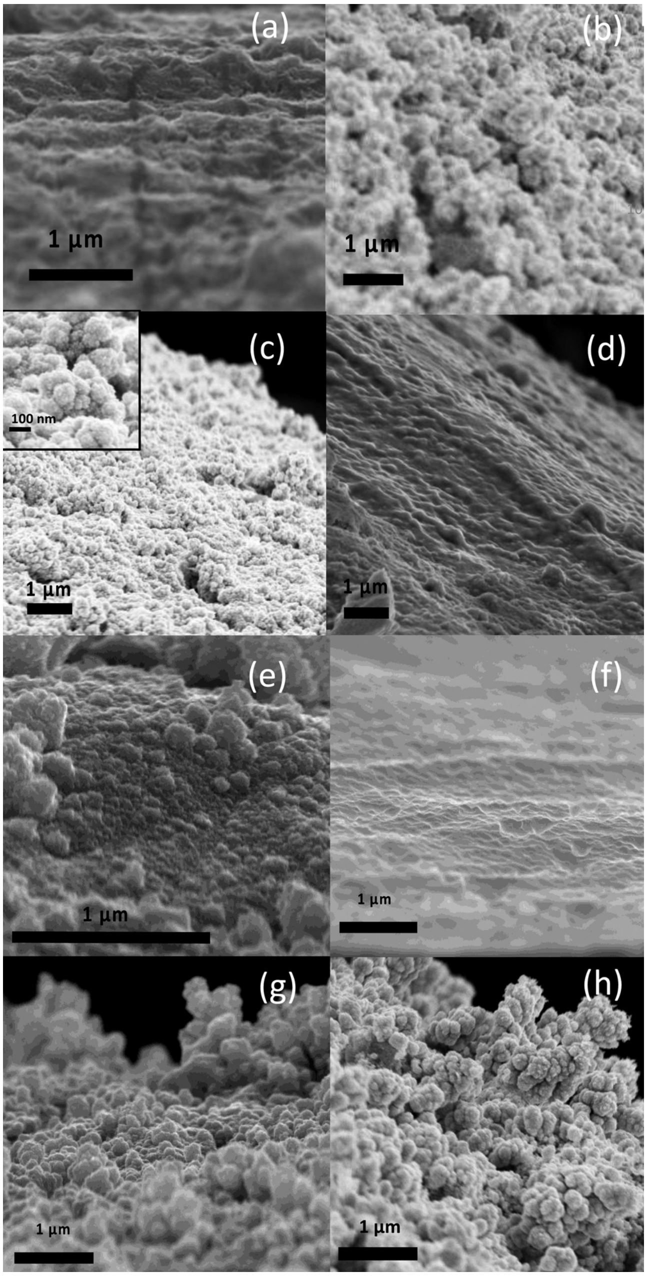

Fig. 2. SEM micrographs of (a) SS/$Pd_{0.2}Sn_{0.8}$-497, (b) SS/$Sn_{0.8}Pd_{0.2}$-497, (c) SS/$Sn_{0.8}Pd_{0.2}$-166, (d) SS/$Sn_{0.8}Pd_{0.2}$-332, (e) SS/$Sn_{0.8}Pd_{0.2}$-1490, (f) SS/$Sn_{0.5}Pd_{0.5}$-497, (g) SS/$Sn_{0.2}Pd_{0.8}$-497, (h) SS/$Sn_{0.2}Pd_{0.8}$-497 after nitrate reduction experiments.

with deionized water, dried under ambient condition, and stored in a nitrogen chamber until uses. The mole fraction, x_i, of the metal catalyst, i.e., Pd or Sn, on the electrode was determined by the following equation:

$$x_i = \frac{(I_i \times t_i)/F}{\Sigma(I_i t_i)/F} = \frac{Q_i/F}{\sum Q_i/F} \tag{2}$$

where Q_i is the total electric charge consumed by the ith species (i.e., Sn or Pd) in coulombs (C), I_i and t_i are the current (A) and deposition time (sec) applied to the ith species, and F is the Faraday constant (96,485 C/eq). All electrodes used in this work were denoted as SS/$Sn_{x_i}Pd_{(1-x_i)}$ -Q, in which Q was the total charge (C = I x t), I was current (A), and t was the deposition time (sec). The validity of Pd to Sn ratio was reasonably assured because the experimental conditions for metal deposition were optimized to ensure 100% current efficiency.

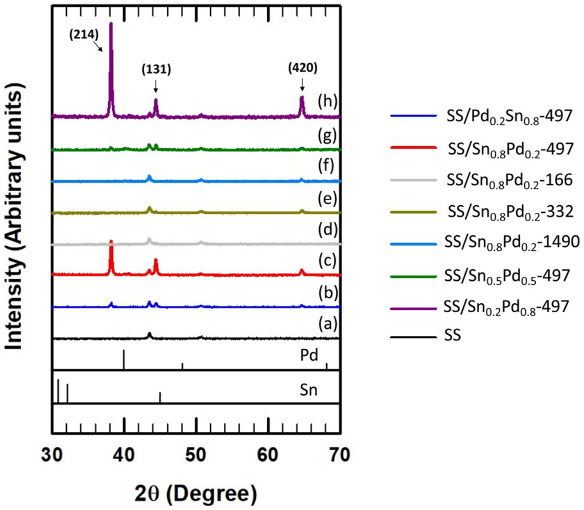

Fig. 3. XRD characterization of (a) SS, (b) SS/$Pd_{0.2}Sn_{0.8}$-497, (c) SS/$Sn_{0.8}Pd_{0.2}$-497, (d) SS/$Sn_{0.8}Pd_{0.2}$-166, (e) SS/$Sn_{0.8}Pd_{0.2}$-332, (f) SS/$Sn_{0.8}Pd_{0.2}$-1490, (g) SS/$Sn_{0.5}Pd_{0.5}$-497, and (h) SS/$Sn_{0.2}Pd_{0.8}$-497. The standard XRD pattern of Pd (PDF # 00-046-1043) and Sn (JCPDS # 04-0673) are also presented for comparison purpose.

To explore the effects of electrode preparation methods on nitrate reduction, three different factors including the sequence of metal deposition, the total electrical charge applied, and Sn-Pd ratio were studied in this work. Electrodes of SS/$Pd_{0.2}Sn_{0.8}$-497 (Sn on the outside surface) and SS/$Sn_{0.8}Pd_{0.2}$-497 (Pd on the outside surface) were studied for the influence of metal deposition sequence on nitrate reduction. The effects of total charge (Q) for electrode deposition on the nitrate reduction were examined by four electrodes prepared with various Q values including SS/$Sn_{0.8}Pd_{0.2}$-166, SS/$Sn_{0.8}Pd_{0.2}$-332, SS/$Sn_{0.8}Pd_{0.2}$-497, and SS/$Sn_{0.8}Pd_{0.2}$-1490. The effects of Sn-Pd ratio were studied using SS/$Sn_{0.8}Pd_{0.2}$-497, SS/$Sn_{0.5}Pd_{0.5}$-497 and SS/$Sn_{0.2}Pd_{0.8}$-497. Prior to each nitrate reduction experiment, the SS/Sn-Pd electrode was regenerated by electrochemical reduction at constant current of 0.05 A for 20 min in pure 0.1 M $HClO_4$ solution as to reduce the divalent tin and palladium ions to their corresponding elemental states, which was confirmed by analyzing the oxidation state of Sn and Pd with XPS before and after the pretreatment (data not shown). Furthermore, there were numeral reports on the electrochemical regeneration of metallic electrodes [52]. Table 1 summarizes detailed preparation conditions for all electrodes in this study.

2.3. Characterization of catalysts

Crystalline Sn-Pd alloy was identified by X-ray diffraction (XRD, Rigaku D-Max B) with Cu Kα radiation at 40 kV beam voltage and 40 mA current, and scan angle from 30° to 70°. The surface element and crystal structure were characterized by matching XRD pattern of each sample to known standard patterns. High resolution transmission electron microscopy (HRTEM, Jeol JEM-2010) was also applied to support the crystal structure determination. HRTEM was operated at 200 kV, and the magnification of HRTEM was 500 K. A small amount of sample was put into the sample tube filled with a 95% ethanol solution. After agitating under an ultrasonic environment for 90 min, one drop of the dispersed slurry was dipped onto a carbon-coated copper mesh (300#) (Ted Pella Inc., CA, U.S.A.) and dried at room temperature in vacuum overnight. Surface morphology and structure of the metal deposits were investigated by a scanning electron microscopy (JSM 7400 F) at an accelerating voltage of 3 kV. Cyclic voltammetry (CV) and linear sweep voltammetry (LSV) were conducted using a three-electrode configuration with an electrochemical workstation (CHI 611).

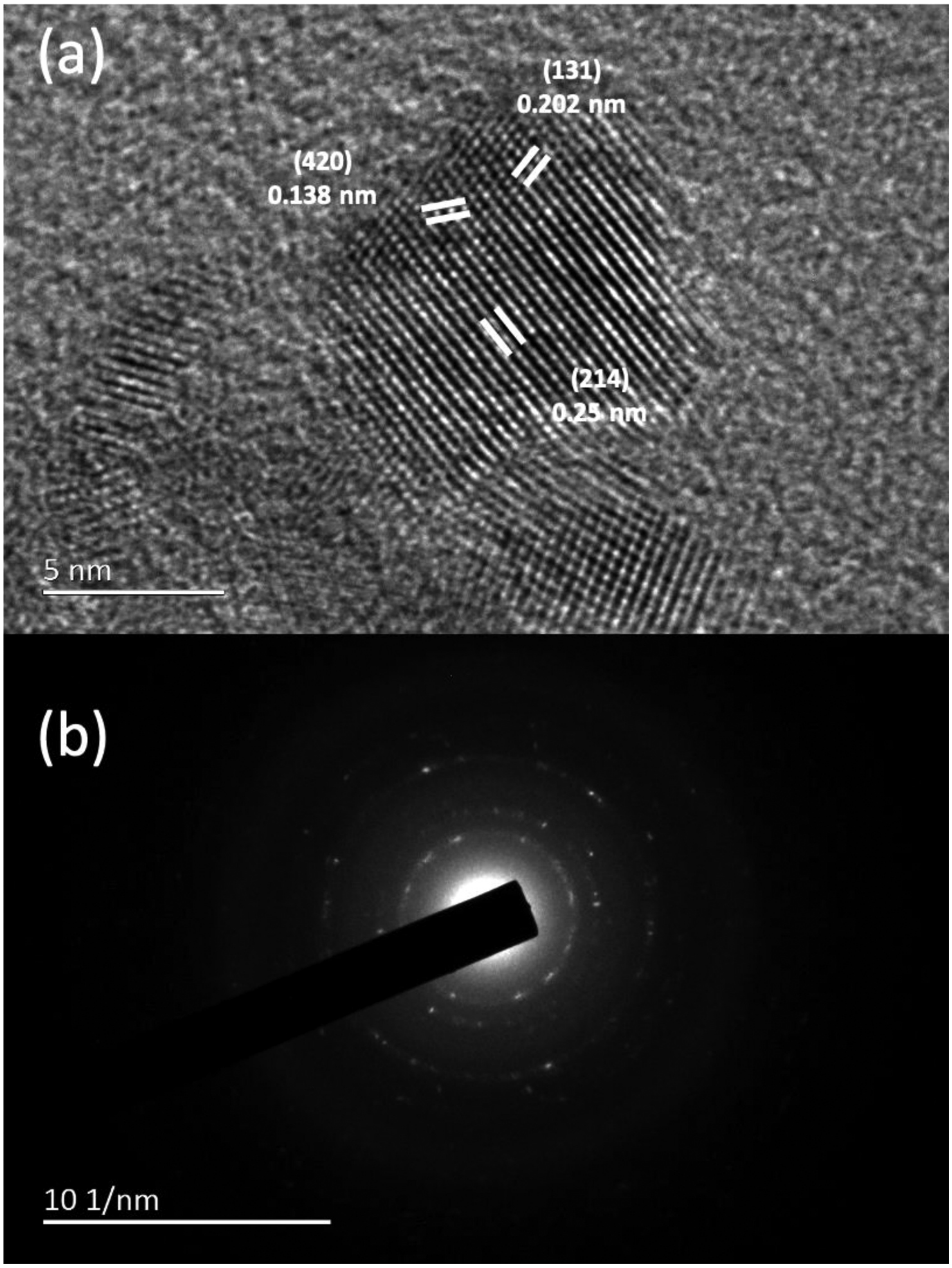

Fig. 4. (a) Representative HRTEM image of SS/$Sn_{0.2}Pd_{0.8}$-497 electrode and (b) corresponding selected-area electron diffraction (SAED) patterns.

The counter and reference electrode used were Pt rod and SCE, respectively. LSV tests were measured in 8.0×10^{-3} M nitrate solution with a scan rate of 10 mV/s from -0.7 to -1.1 V (vs SCE). The electrochemical impedance measurements (EIS) were carried out in the frequency range from 100 kHz to 0.1 Hz with oscillation amplitude of 10 mV/s using a Princeton Applied Research potentiostat/galvanostat (Parstat 2263). The reference electrode was a SCE and all the potential measurements were based on SEC.

2.4. Electrochemical nitrate reduction

Nitrate reduction experiments were performed in a divided two-electrode system, as shown in Fig. 1. Graphite electrode was the anode and SS/Sn-Pd electrode as the cathode. The working solution was 8.0×10^{-3} M of $NaNO_3$ and the current was constant at -0.04 A. The volume of the cathode chamber and anodic chamber were 467 and 500 mL, respectively. An H-type reactor with a cationic membrane partition keeping the cathodic chamber pH low at 1.5. The pH value remained relatively unchanged during the reaction due to the presence of the strong acid in the electrolyzed solution. Nitrate and nitrite were measured with a Dionex ion chromatograph (IC) system equipped with a GP50 pump, ED 40 conductance detector, Dionex IonPac AC20 column (4 mm × 250 mm.), and Dionex AS 40 automatic sampler. The effluent mobile phase was a mixture of deionized water and 50 mM NaOH with a flow rate of 1 mL/min and injection volume of 25 μL. At different time intervals, 3 mL of samples were withdrew withdrawnfrom the electrochemical cell for chemical analysis of related residual nitrogen species. A Dionex ion chromatograph (IC) system equipped with a GP40 pump, CD 20 conductance detector, Dionex IonPac CS16 column (0.5 mm × 250 mm.), and Dionex AS 3500 automatic sampler were used to measure the ammonium concentration. The effluent mobile phase was a mixture of deionized water and 0.1 M of methanesulfonic acid, with a flow rate of 1 mL/min and injection volume of 25 μL. Gaseous products from nitrate reduction reaction were

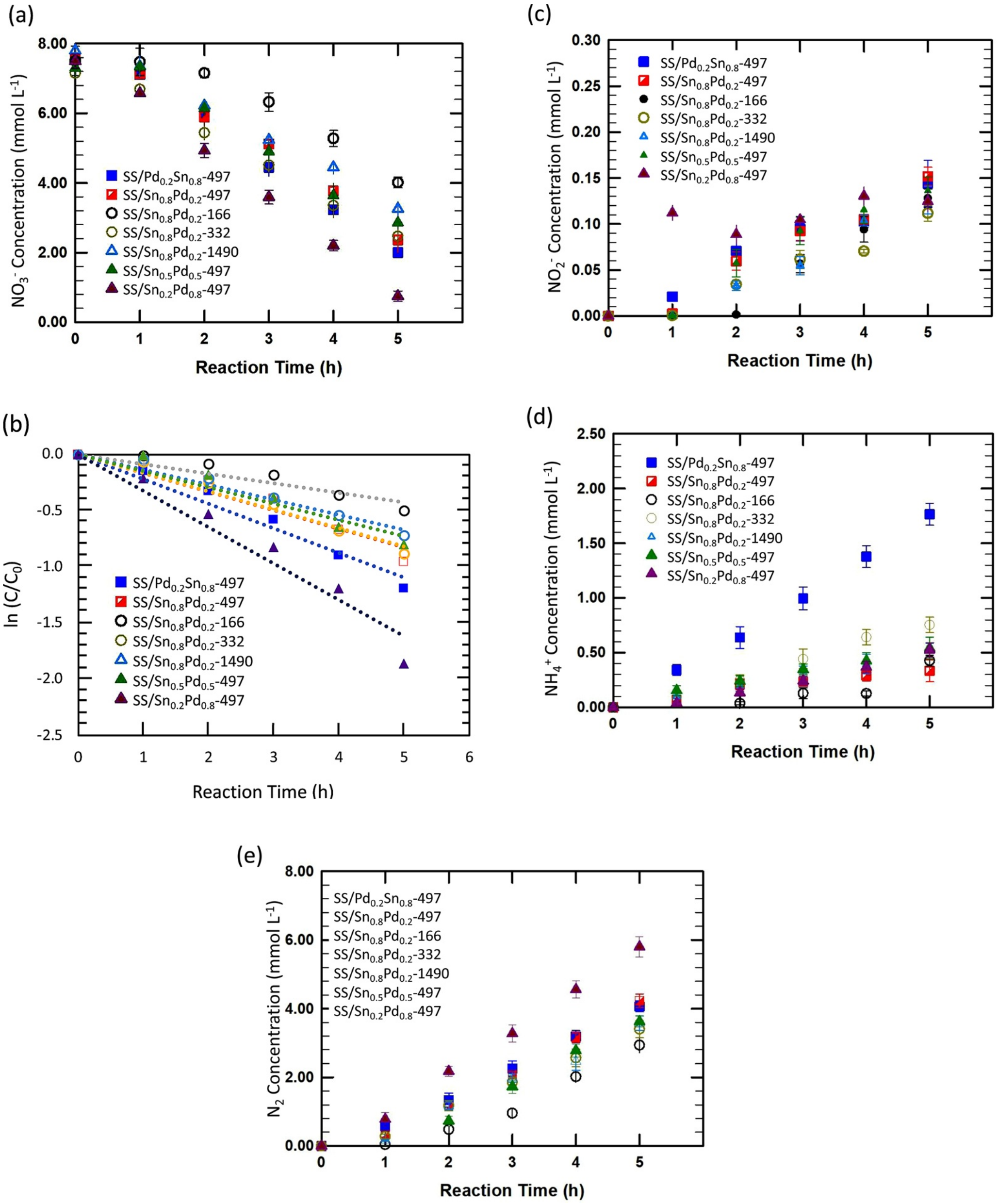

Fig. 5. Nitrate reduction reaction in different electrode systems. (a) Nitrate concentration versus reaction time; (b) The fitting of kinetic model (dash line) and experimental data (dot). (c) Nitrite concentration versus reaction time; (d) Ammonium concentration versus reaction time; (e) Nitrogen concentration versus reaction time. The reported values are averages from three samples with standard deviations indicated by error bars on the data points. Experimental conditions: pH = 1.5; [NaNO$_3$] = 0.008 M; temperature = 25 °C; constant current = -0.04 A; voltage = 5 V to 6 V.

analyzed with GC-MS (HP 6890 series, Agilent Technologies, Santa Clara, USA) equipped with a bonded polystyrene-divinylbenzene based column (HP-PLOT/Q, 15 m x 0.32 mm id). The mass spectrometric analysis was undertaken with a mass selective detector 5973 (Agilent Technologies, Santa Clara, USA). Note that the gaseous nitrous oxide (N$_x$O) was not detected by GC-MS in all experiments. The concentration of N$_2$ was determined by the combination of mass balance and GC-MS. GC-MS was applied mainly to detect the presence of gaseous nitrous oxides (N$_x$O) produced as end products. As the gaseous nitrous oxide (N$_x$O) was not detected by GC-MS in the present work, we assumed that NO$_2^-$, NH$_4^+$, and N$_2$ were main reduction products and thus gaseous nitrogen could be quantified by mass-balance.

Nitrate conversion rate constant, k, was obtained by fitting experimental date with the first-order rate equation as shown in Eq. 3 [22,34]:

$$r = \frac{-d[NO_3^-]_t}{dt} = -k[NO_3^-]_t \quad (3)$$

in which $[NO_3^-]_t$ was the nitrate concentration (mol/L) at reaction time t. The fraction of nitrate conversion, $X_{NO_3^-}$, was calculated by Eq. 4:

$$X_{NO_3^-} = \frac{[NO_3^-]_0 - [NO_3^-]_t}{[NO_3^-]_0} \quad (4)$$

in which $[NO_3^-]_0$ was the initial nitrate concentration. The selectivity of reaction products, i.e., $S_{NO_2^-}$, $S_{NH_4^+}$, and S_{N_2} were calculated by the following equations:

$$S_{NO_2^-} = \frac{[NO_2^-]_t}{[NO_3^-]_0 - [NO_3^-]_t} \quad (5a)$$

$$S_{NH_4^+} = \frac{[NH_4^+]_t}{[NO_3^-]_0 - [NO_3^-]_t} \quad (5b)$$

Table 2
Kinetic constants, nitrate removal, selectivity of nitrite, ammonium, and nitrogen, nitrogen yield, and charge transfer resistance.

Samples	k (h^{-1})	R^2	$X_{NO_3^-}$	$S_{NO_2^-}$	$S_{NH_4^+}$	S_{N_2}	η_{N_2}	R_{ct} (Ω)
SS/$Pd_{0.2}Sn_{0.8}$-497	0.32	0.96	0.74	0.02	0.30	0.68	0.50	32
SS/$Sn_{0.8}Pd_{0.2}$-497	0.24	0.96	0.65	0.03	0.09	0.88	0.58	40
SS/$Sn_{0.8}Pd_{0.2}$-166	0.14	0.91	0.47	0.03	0.13	0.84	0.38	72
SS/$Sn_{0.8}Pd_{0.2}$-332	0.24	0.98	0.63	0.02	0.18	0.80	0.53	41
SS/$Sn_{0.8}Pd_{0.2}$-1490	0.20	0.98	0.56	0.03	0.13	0.84	0.48	59
SS/$Sn_{0.5}Pd_{0.5}$-497	0.22	0.99	0.60	0.03	0.14	0.83	0.50	48
SS/$Sn_{0.2}Pd_{0.8}$-497	0.47	0.92	0.88	0.02	0.09	0.89	0.79	23

1. k = nitrate removal rate constant; R^2 = coefficient of determination; $X_{NO_3^-}$ = nitrate conversion; $S_{NO_2^-}$, $S_{NH_4^+}$, S_{N_2} = selectivity of NO_2^-, NH_4^+, and N_2; η_{N_2} = nitrogen yield; R_{ct} = charge transfer resistance.

2. Example electrode identification: SS/$Pd_{0.2}Sn_{0.8}$-497 = 20% Pd right on the SS surface and 80% Sn on the outside surface prepared with total charge of 497C.

$$S_{N_2} = \frac{[NO_3^-]_0 - [NO_3^-]_t - [NO_2^-]_t - [NH_4^+]_t}{[NO_3^-]_0 - [NO_3^-]_t} \tag{5c}$$

in which $[NO_2^-]_t$ and $[NH_4^+]_t$ were the concentration of nitrite and ammonium, respectively, at time t.

3. Results and discussion

3.1. Characterization of synthesized bimetallic electrodes

Fig. 2 shows the surface morphology of electrodes characterized by SEM. Fig. 2a and b are the SEM micrographs of SS/$Pd_{0.2}Sn_{0.8}$-497 (Sn on the outer layers) and SS/$Sn_{0.8}Pd_{0.2}$-497 (Pd on the outer layers), respectively. It is clear that the electrode surface of SS/$Sn_{0.8}Pd_{0.2}$-497 composed of multiple nanoparticles, leading to higher roughness compared to the surface of SS/$Pd_{0.2}Sn_{0.8}$-497. Fig. 2b-2e represent the SEM micrographs of four electrodes prepared with different Q values, exhibited distinct surface architectures among all four electrodes. Although these four electrodes appeared to compose nanoparticles on the surface, the degree of roughness was clearly different. Considering that all samples have the same composition and deposition sequence, we postulate that different Q applied resulted in different electrode surface properties. SEM micrographs of Fig. 2b, f, g reveal the surface morphologies of electrodes prepared from different Sn to Pd ratios. It is noted that the roughness features of SS/$Sn_{0.8}Pd_{0.2}$-497 (Fig. 2b) and SS/$Sn_{0.2}Pd_{0.8}$-497 (Fig. 2g) are much more pronounced than that of the SS/$Sn_{0.5}Pd_{0.5}$-497 electrode (Fig. 2f). Fig. 2h shows the SEM micrograph of SS/$Sn_{0.2}Pd_{0.8}$-497 after nitrate reduction experiment. The similar features between Fig. 2g and h indicate the surface structure was retained, demonstrating the stability of Sn-Pd bimetallic electrodes prepared in this study.

The surface morphology of electrodes was also characterized by XRD as shown in Fig. 3. Note that the major diffraction peaks of Pd metal were located at 2θ = 40, 48, and 68 with (111), (200), and (220) crystal facets, respectively (ICDD PDF Card No. 00-046-1043) [53–55]. The major diffraction peaks of Sn metal were located at 2θ = 30.7, 32, and 45 with (200), (101), and (211) crystal facets, respectively (JCPDS Card No. 04-0673) [55–57]. The surface crystal structure was assigned by matching XRD pattern of each sample with known standard patterns [31,58–60]. Interestingly, most samples exhibited X-ray diffraction peaks at 2θ = 38.1, 44.4, and 64.6, excluding 2θ = 43.5, 50.8 from the stainless steel (ICDD PDF Card No. 00-033-0397), indicating the formation of Sn_3Pd alloy (ICDD PDF Card No. 00-015-0575) with (214), (131), and (420) crystal facets on the electrode surface, respectively. In some cases, such as SS/$Sn_{0.8}Pd_{0.2}$-166, the crystal structure was presumed to be Sn_3Pd alloy based on metal composition because the diffraction peaks at 2θ = 38.1 and 64.6 were indistinguishable from the noise. The result indicated that the orientation of facets (214) and (420) of the electrode were not paralleled to the sample surface [58,60,61]. The intensity of all XRD patterns were normalized against stainless steel support, the variance in peak intensity among electrodes suggested that the electrodeposition procedure influenced the preferred orientation for the growth of crystallites as well as crystal facet distribution. Fig. 4 gives the HRTEM image and the corresponding selected-area electron diffraction (SAED) patterns of SS/Sn0.2Pd0.8-497 electrode. Results showed three strong continuous lattice fringes with lattice spacing of 0.250 nm, 0.202 nm, and 0.138 nm. Note that the spacing calculated from SAED pattern matched the d-spacing of the (214), (131), and (420) plane in Sn3Pd phase (i.e. 0.240 nm, 0.204 nm, and 0.145 nm, respectively, according to ICDD PDF Card No. 00-015-0575). The result was consistent with XRD characterization, supporting the formation of Sn3Pd alloy.

3.2. Optimizing electrode preparation procedures

Fig. 5 shows the concentration change of NO_3^-, NO_2^-, NH_4^+, and N_2 as a function of reaction time at constant current of $^-$0.04 A. Results present in Fig. 5a indicated that nitrate was readily electrochemically reduced over all SS/Sn-Pd electrodes. Table 2 gives the kinetic constant of NO_3^- reduction over seven different electrodes. The kinetic analysis revealed that NO_3^- reduction follow the first-order-kinetic model ($R^2 > 0.91$) as shown in Fig. 5b. Electrode with Pd on the outside surface, i.e., SS/$Sn_{0.2}Pd_{0.8}$-497 exhibited relatively greater nitrate removal rate constant and nitrate conversion (k = 0.47 h^{-1}, $X_{NO_3^-}$ = 0.88) than that with Sn deposited on the outside of the electrode, i.e., SS/$Pd_{0.8}Sn_{0.2}$-497 (k = 0.24 h^{-1}, $X_{NO_3^-}$ = 0.65) under otherwise identical conditions, indicating electrodes with Sn-rich outer surface was beneficial to nitrate conversion.

For electrodes prepared with same Sn to Pd ratio (SS/$Sn_{0.8}Pd_{0.2}$) but different Q, it appeared that nitrate conversion increased with increasing Q, reached maximum value at Q of approximately 500 C then slightly tailed off. The removal rate constant also revealed the same trend with low k on SS/$Sn_{0.8}Pd_{0.2}$-166 (k = 0.14 h^{-1}) and maintaining constant k value (k = 0.24 h^{-1}) on SS/$Sn_{0.8}Pd_{0.2}$-332 and SS/$Sn_{0.8}Pd_{0.2}$-497, except a slight drop of k on SS/$Sn_{0.8}Pd_{0.2}$-1490 (k = 0.20 h^{-1}).

For electrodes with the same Q of 497 C, but different Sn to Pd ratios, namely, SS/$Sn_{0.2}Pd_{0.8}$-497, SS/$Sn_{0.5}Pd_{0.5}$-497, and SS/$Sn_{0.8}Pd_{0.2}$-497, nitrate conversion decreased from 0.88 at Sn:Pd = 1:4 to 0.60 at Sn:Pd = 1:1 then increased to 0.65 at Sn:Pd = 4:1, while k (h^{-1}) decreased from 0.47 at Sn:Pd = 1:4 to 0.22 at Sn:Pd = 1:1 then increased to 0.24 at Sn:Pd = 4:1. The SS/$Sn_{0.2}Pd_{0.8}$-497 electrode exhibited the highest nitrate conversion among all bimetallic electrodes in this work, indicating Sn:Pd metal ratio of 1:4 was sufficient for the reduction of most nitrate ions in the solution. Further increase in Sn loading might block Pd active sites and reduce the reaction rate and selectivity [49,50,61].

Fig. 5c shows the variation of nitrite concentration versus reaction time. In general, nitrite concentration increased with reaction time. After 5 h, nitrite concentration and selectivity were low, indicating no nitrite accumulation and fast reaction kinetics [62]. Fig. 5d gives the concentration of ammonium as a function of reaction time. Results again showed the importance of the deposition sequence of metals on ammonium selectivity. Interestingly, ammonium selectivity was inhibited when Pd was deposited after Sn, i.e., Pd was on the outer layers of the electrode structure. All electrodes prepared by depositing Sn first then Pd (SS/Sn-Pd) exhibited low NH_4^+ production, which might be resulted from insufficient surface hydrogen on Pd sites and thus weakening hydrogenation abilities due to the blockage of Pd active sites by Sn metal. According to Eqs. (1c)–(1f), hydrogenation from Pd[H] strongly participated in the nitrate reduction pathway toward N_2 formation. In the case of SS/$Pd_{0.2}Sn_{0.8}$-497, Pd[H] might not be enough in density or availability for the overall reaction as the active sites were covered or blocked by Sn. Thus, the reduced N-intermediates from

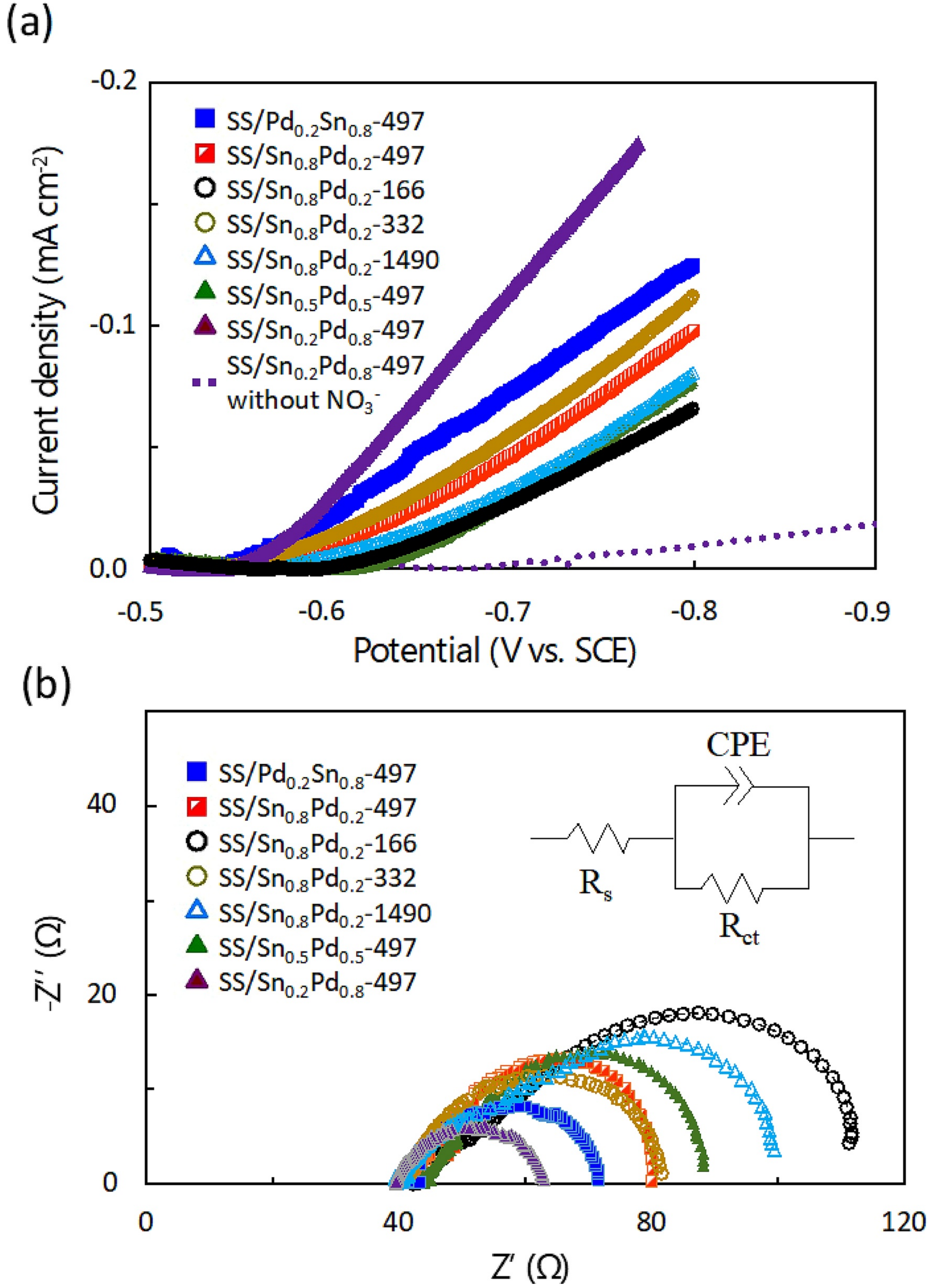

Fig. 6. Electrochemical characterization for different electrode systems. (a) Polarization curve from linear sweep voltammetry; (b) Nyquist plot from electrochemical impedance spectroscopy with equivalent circuit fitting in the inset. Experimental conditions: pH = 1.5; [NaNO$_3$] = 0.008 M; temperature = 25 °C; constant current = -0.04 A; voltage = 5 V to 6 V.

nitrate were not able to pair with the two nearby N-species and form N_2, which led to increase in the production of NH_4^+ end products [50,63].

Fig. 5e shows N_2 concentration as a function of reaction time. SS/Sn$_{0.2}$Pd$_{0.8}$-497 exhibited superior N_2 selectivity over SS/Pd$_{0.8}$Sn$_{0.2}$-497, which again demonstrated the importance of metal deposition sequence; Pd on the outer layer of electrode structure displayed higher nitrogen production. N_2 selectivity (S_{N_2}) was 0.84, 0.80, 0.88, and 0.84 on SS/Sn$_{0.8}$Pd$_{0.2}$-166, SS/Sn$_{0.8}$Pd$_{0.2}$-332, SS/Sn$_{0.8}$Pd$_{0.2}$-497, and SS/Sn$_{0.8}$Pd$_{0.2}$-1490, respectively.

Table 3
Comparison of nitrogen selectivity by catalytic electrochemical nitrate reduction.

Cathode Material	Support	Cathode Source	Cell Type	Experimental Conditions	NH_4^+ yield (%)	N_2 yield (%)	Ref.
Cu	N/A	Commercial	Undivided	pH = 12 0.1 M $NaNO_3$ 0.01 M NaOH 0.5 M NaCl I = 0.6 mA	26.4	30	[36]
Al	N/A	Commercial	Divided	− 1.8 V (vs. Ag/AgCl)	47	38.1	[25]
Pb	N/A	Commercial	Divided	− 2.0 V (vs. Ag/AgCl)	64	16	[25]
$Cu_{0.6}Zn_{0.4}$	N/A	Commercial	Divided	− 0.5 V (vs. Ag/AgCl)	75	2.08	[25]
$Sn_{0.85}Cu_{0.15}$	N/A	Commercial	Divided	− 1.6 V (vs. Ag/AgCl)	2	7.6	[25]
$Sn_{0.85}Cu_{0.15}$	N/A	Commercial	Divided	− 2.0 V (vs. Ag/AgCl)	40	34.4	[25]
$Pd_{0.4}Cu_{0.6}$	Ni	Electro-deposition	Undivided	pH = 7 50 ppm $NaNO_3$ − 0.3 V (vs. SCE)	49	41	[31]
$Pd_{0.62}Cu_{0.38}$	Stainless Steel	Electro-deposition	Divided	0.1 M $NaNO_3$ 1 M NaOH − 0.93 V (vs. SCE)	10	76	[32]
$Pd_{0.82}Sn_{0.18}$	Activated carbon fiber	Electro-deposition	Divided	pH = 5 0.002 M $NaNO_3$ 3.2 − 4.2 V (vs. SCE) I = -0.04 A	9	80	[65]
Pd/Sn	Au	Adsorption	Divided	0.01 M $NaNO_3$ 0.1 M $HClO_4$	6.8	21	[52]
Sn-Pd	Red mud	Impregnation	Undivided	0.0005 M $NaNO_3$ H_2/CO_2 gas supply	10	88	[55]
Blended $Sn_{0.8}Pd_{0.2}$	Stainless Steel	Electro-deposition	Divided	pH = 1.5 0.008 M $NaNO_3$ 0.1 M $HClO_4$ I = -0.04 A	14	81	[34]
$Sn_{0.2}Pd_{0.8}$	Stainless Steel	Electro-deposition	Divided	pH = 1.5 0.008 M $NaNO_3$ 0.1 M $HClO_4$ I = -0.04 A	7.9	79	This work

In terms of Sn to Pd ratio, the N_2 selectivity (S_{N_2}) was decreased from 0.88 at Sn:Pd = 4:1 (SS/$Sn_{0.8}Pd_{0.2}$-497) to 0.83 at Sn:Pd = 1:1 (SS/$Sn_{0.5}Pd_{0.5}$-497) then increased to 0.89 at Sn:Pd = 1:4 (SS/$Sn_{0.2}Pd_{0.8}$-497). It was noted that all SS/Sn-Pd electrodes, except SS/$Pd_{0.2}Sn_{0.8}$-497, achieved high N_2 selectivity (> 0.80), which supported above argument that the availability and accessibility of Pd[H] during nitrate reduction were critical to N_2 formation process.

Note that the nitrate reduction toward N_2 generation can be expressed as well in terms of N_2 yield (η_{N_2}), which is the product of nitrate conversion ($X_{NO_3^-}$) and nitrogen selectivity (S_{N_2}) using Eq. 6:

$$\eta_{N_2} = X_{NO_3^-} \times S_{N_2} \tag{6}$$

Table 2 showed the effects of electrode preparation procedure on the selectivity of several major products, including nitrate ($S_{NO_2^-}$), ammonium ($S_{NH_4^+}$) and nitrogen molecule (S_{N_2}), and nitrogen yield (η_{N_2}). In terms of metal deposition sequence, the difference in η_{N_2} between Sn and Pd was only 8% (0.58 for SS/$Sn_{0.8}Pd_{0.2}$-497 versus 0.50 for SS/$Pd_{0.2}Sn_{0.8}$-497). At Q of 166, i.e., the SS/$Sn_{0.8}Pd_{0.2}$-166 electrode exhibited the lowest N_2 yield ($\eta_{N_2} = 0.38$) among all electrodes studied. With respect to metal ratio, nitrogen yield decreased from 0.79 at Sn:Pd = 1:4 to 0.50 at Sn:Pd = 1:1 then increased to 0.58 at Sn:Pd = 4:1. Results showed that the electrode prepared at Sn:Pd ratio of 1:4 (SS/$Sn_{0.2}Pd_{0.8}$-497) exhibited the largest nitrate removal rate constant ($k = 0.47\,h^{-1}$), nitrate conversion ($X_{NO_3^-} = 0.88$), N_2 selectivity (S_{N_2}= 0.89), and N_2 yield (η_{N_2}= 0.79) than all other SS/Sn-Pd electrodes in this work (Table 2). As all electrodes with Pd deposition on the outside surface exhibiting similar N_2 selectivity due to sufficient Pd[H] for the reduction reaction. The superior N_2 yield on SS/$Sn_{0.2}Pd_{0.8}$-497 could be attributed to its outstanding nitrate conversion, which was resulted from optimal metal ratio as discussed above.

CV and LSV characterized the electrochemical behavior of electrodes prepared in this study as shown in Fig. S1 and Fig. 6a, respectively. Results of CV analysis showed that different preparation parameters influenced the cathodic behavior of electrode. Thus, LSV test was applied to verify the performance of different electrodes in nitrate reduction reaction (Fig. 6a). The dash line was the LSV curve of SS/$Sn_{0.2}Pd_{0.8}$-497 without nitrate ion. Subtracting the current density in the absence of nitrate from that in the presence of nitrate gave the net nitrate reduction current [28,65]. Accordingly, the net current density of nitrate reduction followed the order of SS/$Sn_{0.2}Pd_{0.8}$-497 > SS/$Pd_{0.2}Sn_{0.8}$-497 > SS/$Sn_{0.8}Pd_{0.2}$-332 > SS/$Sn_{0.8}Pd_{0.2}$-497 > SS/$Sn_{0.5}Pd_{0.5}$-497 ≈ SS/$Sn_{0.8}Pd_{0.2}$-1490 > SS/$Sn_{0.8}Pd_{0.2}$-166, suggesting that the SS/$Sn_{0.2}Pd_{0.8}$-497 electrode had superior electrochemical activity to all other bimetallic electrodes prepared in this study.

A series of EIS experiments were also conducted on different Sn-Pd electrodes in nitrate solution as to study the charge transfer kinetics. The Nyquist plot was obtained as shown in Fig. 6b, and the corresponding equivalent circuit that fitted the electrochemical system was provided in the inset of Fig. 6b. The simple equivalent circuit consisted of a solution resistance, R_s, a constant phase element, CPE, and a charge transfer resistance, R_{ct}. The impedance of CPE can be expressed as Eq. 7 [64].

$$Z_{CPE} = \frac{1}{(CPET)(i \times w)^n} \tag{7}$$

where CPET is the pre-factor of CPE, i is the imaginary unit, w is the angular frequency, and n is the exponent. The exponent n is a constant value between 0 and 1, and it determines the degree of deviation from an ideal semicircle in Nyquist plot. In the case of $n = 1$, CPE is an ideal capacitor, and CPE describes a pure resistor in the case of $n = 0$ [64]. The EIS parameters including R_s, CPET, and n are listed in Table S1, and the values of R_{ct} are provided in Table 2. It could be noticed that the n value of all electrochemical systems were around 0.64, which explained the depressed semicircle observed in Fig. 6b and suggested the pseudocapacitive behavior of CPE. R_{ct} was calculated from the diameter of semicircle in Nyquist plot. The smaller R_{ct} value indicated faster kinetics in the electron transfer process at the electrode and electrolyte interface. In the present study, R_{ct} was in the order of SS/$Sn_{0.2}Pd_{0.8}$-

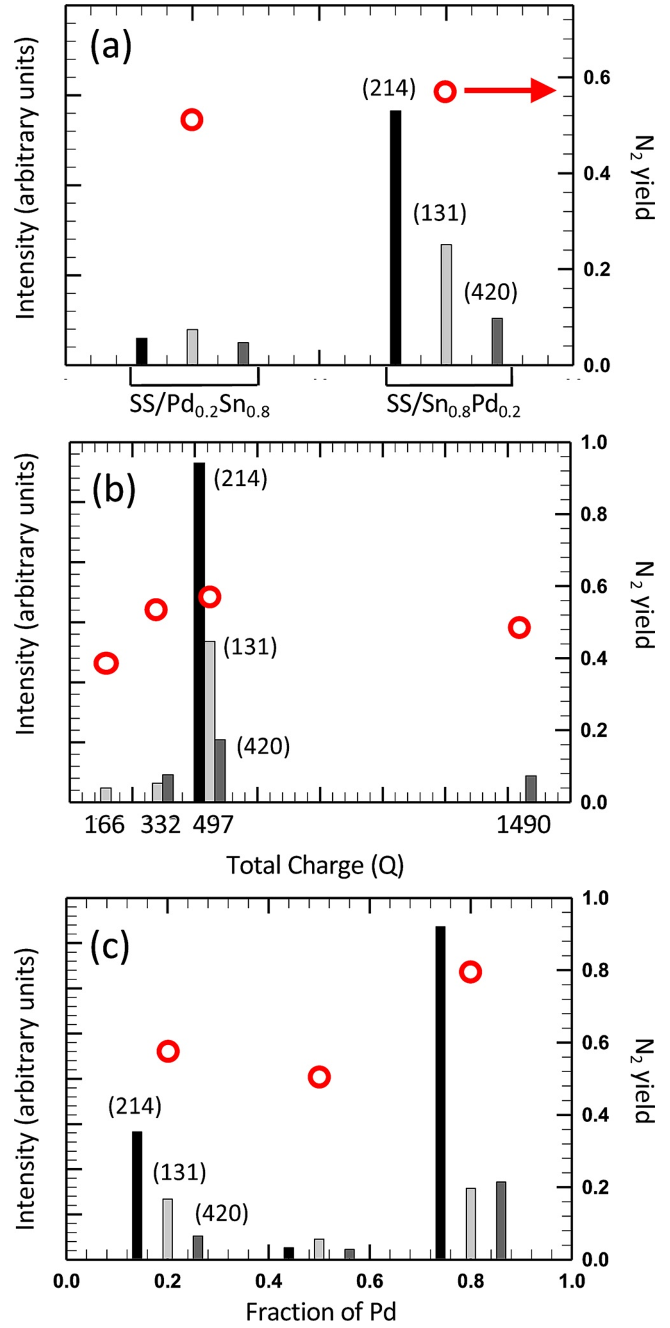

Fig. 7. The relationship among XRD peak intensity, nitrogen yield (open circles), and (a) electrode deposition sequence, (b) total charge for electrode preparation, and (c) fraction of Pd in Sn-Pd electrodes.

497 < $SS/Pd_{0.2}Sn_{0.8}$-497 < $SS/Sn_{0.8}Pd_{0.2}$-497 < $SS/Sn_{0.8}Pd_{0.2}$-332 < $SS/Sn_{0.5}Pd_{0.5}$-497 < $SS/Sn_{0.8}Pd_{0.2}$-1490 < $SS/Sn_{0.8}Pd_{0.2}$-166. The EIS result was in agreement with that of LSV analysis and nitrate conversion data, which confirmed tat $SS/Sn_{0.2}Pd_{0.8}$-497 was superior with respect to electrochemical activity toward nitrate reduction reaction. Additionally, the N_2 yield on $SS/Sn_{0.2}Pd_{0.8}$-497 was also relatively higher than most reported catalytic electrodes in the literature especially in electrochemical nitrate reduction, while NH_4^+ yield remained relatively low at 7.9% (Table 3) [25,31,32,65].

It was further noted that all synthesized electrodes exhibited the same Sn_3Pd XRD pattern (Fig. 3). The major difference among all XRD spectra was the peak intensity. The variance in XRD peak intensity suggested that Sn_3Pd alloy on the electrode surface was composed of different crystal facet distribution. As described in the Introduction section, different crystal facet distribution was known to impact surface active sites responsible for the catalytic reactivity and product selectivity. Therefore, the reactivity and selectivity of electrode $SS/Sn_{0.2}Pd_{0.8}$-497 might also influenced by the modified surface structure of alloy catalyst.

3.3. Effects of surface structure

Fig. 7 shows the relationship between electrode preparation procedures, i.e., metal deposition sequence (Fig. 7a), charge applied (Fig. 7b), and Pd content (Fig. 7c), on N_2 yield (open read circles) with respect to crystal facets, namely, Sn_3Pd(214), Sn_3Pd(131), and Sn_3Pd(420), respectively. Facet peak intensity mostly reflected nitrogen yield. Generally, nitrogen yield correlated well to the XRD peak intensity of crystal facets (Fig. 7a, 7b, and 7c). To elucidate the influence of individual crystal facet on nitrate reduction, the N_2 yield was plotted as a function of peak intensity of the three facets, i.e., Sn_3Pd(214), Sn_3Pd(131) and Sn_3Pd(420), respectively (Fig. 8). The correlation between N_2 yield and peak intensity was evaluated by the Pearson correlation coefficient according to Eq. 7:

$$r = \frac{\sum (x_i - \bar{x})(y_i - \bar{y})}{\sqrt{\sum (x_i - \bar{x})^2}\sqrt{\sum (y_i - \bar{y})^2}} \tag{8}$$

Where r is the linear correlation coefficient, x is the XRD peak intensity of electrode i, y is the N_2 yield of electrode i, and $\bar{x}$ and $\bar{y}$ are the average values of x and y, respectively. The linear correlation coefficient, r, measures the strength of a linear relationship between two variables. The value of r is always between -1 and +1, which means total negative linear correlation and total positive linear correlation, respectively. Table 4 shows that the largest r value was 0.77 for the Sn_3Pd(420) facet (peak at $2\theta = 64.5$) (Fig. 8), which was 10% and 19% higher than Sn_3Pd(131) facet and Sn_3Pd(214) facet, respectively, indicating Sn_3Pd(420) had stronger impact than the other two facets on N_2 yield.

To evaluate the effects of crystal facets on nitrogen yield, the Sn_3Pd crystal structure, i.e. Cmca space group symmetry, identified from XRD results was imported to MERCURY software for 3D structure visualization. Fig. 9 shows the coordination characteristics of Sn_3Pd(214), Sn_3Pd(131), and Sn_3Pd(420) generated by MERCURY simulation. It can be seen that the Sn_3Pd(214) and Sn_3Pd(131) (Fig. 9a, d and b, e, respectively) exhibited undesired diamond-shaped surface atom arrangements [44,66]. On the other hand, Sn_3Pd(420) facet (Fig. 9c, f) hadmainly periodic and rectangular active sites.This particular four-atom surface arrangement is known to offer optimal electronic and/or coordination conditions for outstanding electro-catalytic activity as exemplified by oxygen reduction reaction on Au(100) [67,68], CO_2 reduction to ethylene on Cu(100) [69], the oxidation of ammonia on Pt (100) [70,9,71], and the reduction of nitrate on Pt(100) [43,45].

Based on the above observation, mechanism for nitrate reduction on Sn_3Pd(420) facet was attempted (Fig. 10a) as follows. The main feature of the proposed reaction mechanism (Fig.10a) are: (1) adsorption of nitrate ion onto an empty Sn site via oxygen atom; (2) adsorption of hydrogen on the empty Pd site; (3) bond breaking between N and OH; (4) bond breaking between N and O; (5) bond formation between adjacent two N atoms; (6) final bond breaking between N and O, leading to the formation of N_2. As shown in Figs. 10b and 10c, the adsorption of hydrogen on Pd and bond breaking between N and OH were difficult on Sn_3Pd(214) and Sn_3Pd(131) facets likely due to steric restrictions. The result revealed that surface structure design of bimetallic alloy could be applied to modify the hydrogenation ability of catalyst, enabling a unique control over nitrate reduction mechanism.

In summary, results demonstrated that manipulating electrode preparation procedures could impact the nitrate conversion and N_2 selectivity due to the availability of surface hydrogen on Pd for reduction reactions. Additionally, modifying electrode preparation

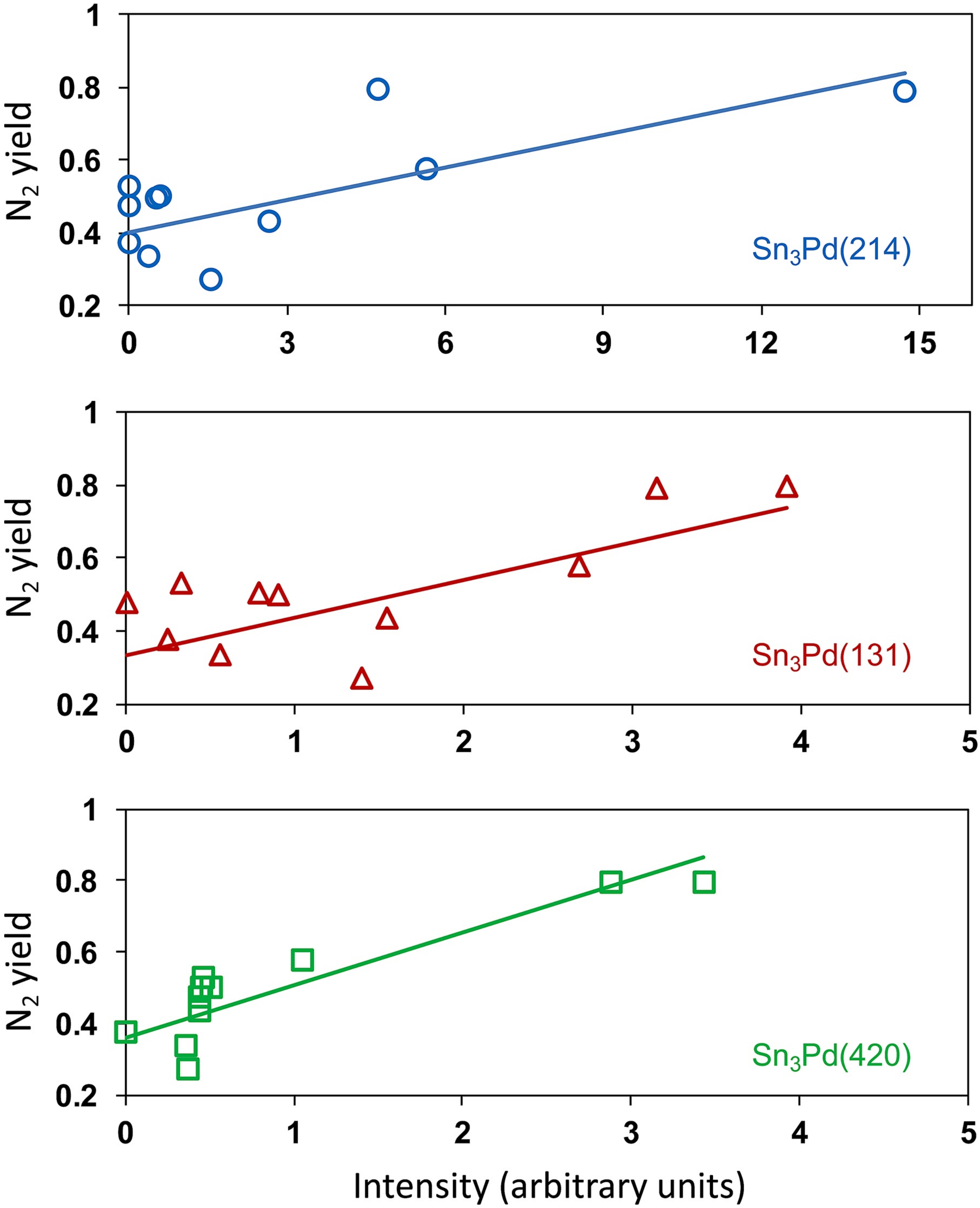

Fig. 8. Relationship between nitrogen yield and crystal facets. Solid line was included for visual clarity.

Table 4
Values of correlation coefficient for three crystal facets.

Crystal Facet	*r*
$Sn_3Pd(214)$	0.65
$Sn_3Pd(131)$	0.70
$Sn_3Pd(420)$	0.77

r: linear correlation coefficient.

procedures also changed crystal facet distribution on the electrode surface, which was found to influence nitrate reduction products. Different surface atom arrangements of bimetallic alloy on electrodes and associated several bond-breaking and bond-forming events contributed to nitrate reactivity and selectivity. The protocol highlighted herein could be extended to other electro-catalytic reactions relevant to the nitrogen cycle specifically and be employed to synthesize different bimetallic electrodes with optimal surface-atomic structure and hydrogenation ability, for promoting applications in the fields of wastewater treatment, electrochemical sensors, electrochemical synthesis, and energy conversion.

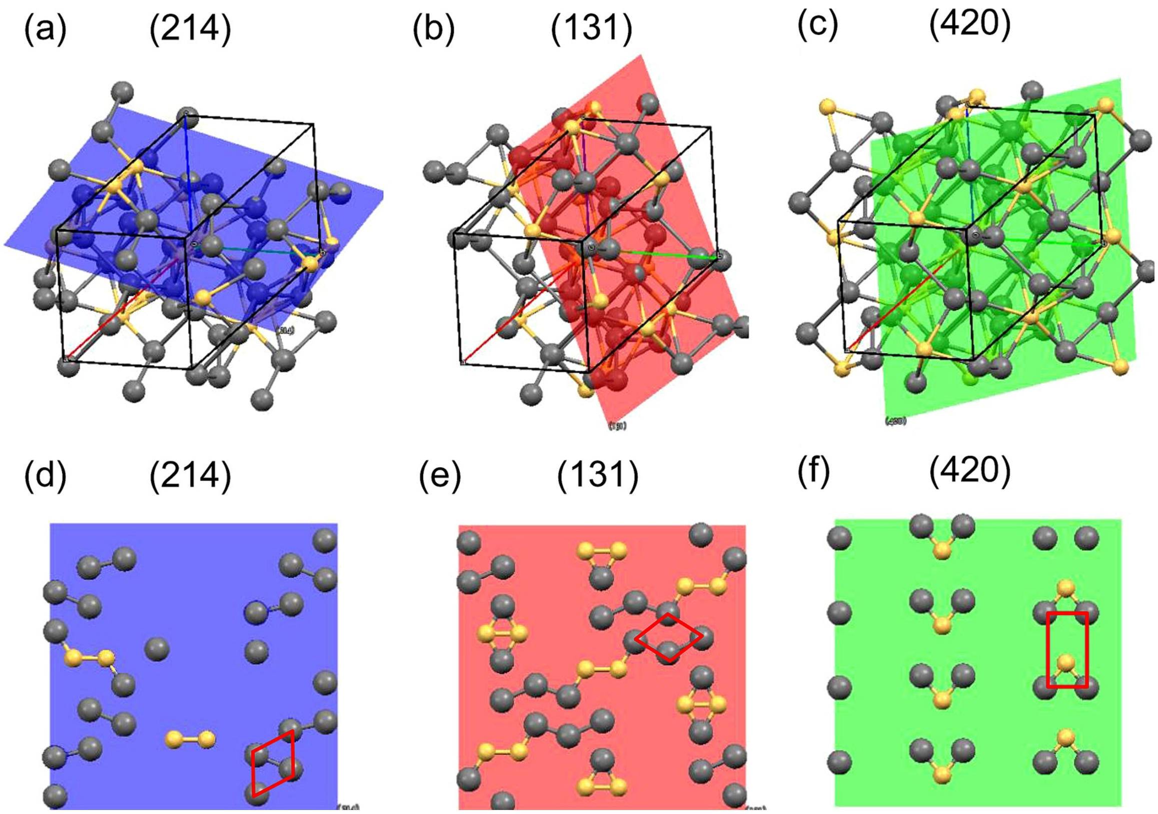

Fig. 9. MERCURY simulation of Sn_3Pd crystal phase with (a) Sn_3Pd(214), (b) Sn_3Pd(131), and (c) Sn_3Pd(420). (d) Perpendicular view to Sn_3Pd(214) facet; (e) Perpendicular view to Sn_3Pd(131) facet; (f) Perpendicular view to Sn_3Pd(420) facet. Diamond-shape and rectangular atom structures are highlighted by red lines. It can be seen that undesired diamond-shaped surface atom arrangement appears on the Sn_3Pd(214) and Sn_3Pd(131) (a, d and b, e). On the other hand, the plane of Sn_3Pd(420) contains mainly periodic and rectangular active sites, which is favorable for the bond-breaking reaction (For interpretation of the references to colour in this figure legend, the reader is referred to the web version of this article).

4. Conclusion

Bimetallic electro-catalyst preparation procedure affected the crystal structure and hydrogenation ability of the catalysts, which in turn, governed nitrate reduction reactivity and N_2 selectivity. The sequence of deposition of the two metals, namely, Pd and Sn, (i.e., deposition sequence), total electrical charge applied for electrode preparation, and molar ratio of the bimetal together could influence the availability of surface hydrogen on catalyst as well as the intensity of the preferred crystal facet orientation, thereby affecting nitrate reduction performance over the SS/Sn-Pd electrode. Results from simple analysis of reaction products, SEM, TEM, and XRD revealed that the crystal facet distribution played a critical role in the nitrate reduction reaction. Specifically, among the three major facets, Sn_3Pd(210), Sn_3Pd(131), and Sn_3Pd(420), Sn_3Pd(420) exhibited the highest N_2 yield, which was likely due to the favorable arrangement of active sites for nitrate adsorption and subsequent bond breaking and formation reactions. Electrode prepared by depositing tin then palladium at tin to palladium atomic ratio of 1:4 and with 497 C applied charge, namely, the SS/$Sn_{0.2}Pd_{0.8}$-497 electrode exhibited the best performance in nitrate reactivity and dinitrogen selectivity/yield, with 88%, 89% and 79% of total nitrate removal, dinitrogen selectivity and yield, respectively. Results of LSV analysis gave the net nitrate reduction current density in the order: SS/$Sn_{0.2}Pd_{0.8}$-497 > SS/$Pd_{0.2}Sn_{0.8}$-497 > SS/$Sn_{0.8}Pd_{0.2}$-332 > SS/$Sn_{0.8}Pd_{0.2}$-497 > SS/$Sn_{0.5}Pd_{0.5}$-497 ≈ SS/$Sn_{0.8}Pd_{0.2}$-1490 > SS/$Sn_{0.8}Pd_{0.2}$-166. EIS analysis showed that Rct value followed the order of SS/$Sn_{0.2}Pd_{0.8}$-497 < SS/$Pd_{0.2}Sn_{0.8}$-497 < SS/$Sn_{0.8}Pd_{0.2}$-497 < SS/$Sn_{0.8}Pd_{0.2}$-332 < SS/$Sn_{0.5}Pd_{0.5}$-497 < SS/$Sn_{0.8}Pd_{0.2}$-1490 < SS/$Sn_{0.8}Pd_{0.2}$-166. The EIS result was in agreement with that of LSV analysis and nitrate conversion data, which confirmed tat SS/$Sn_{0.2}Pd_{0.8}$-497. Results observed in this study, i.e., direct nitrate reduction rate, LSV and EIS measurements, clearly indicated that SS/$Sn_{0.2}Pd_{0.8}$-497 was superior with respect to electrochemical activity toward nitrate reduction reaction. Manipulating electrode synthesis procedure enables control the crystal facet distribution of bimetallic electrodes, leading to enhanced electrochemical nitrate reduction. The findings highlighted herein will allow for the design and synthesis of desirable surface-atomic structure and provide strategy toward fabricating efficient and cost-effective electrodes for electrochemical denitrification in water treatment process.

CRediT authorship contribution statement

Jenn Fang Su: Writing - original draft, Formal analysis, Resources. **Wei-Fan Kuan:** Resources. **Ching-Lung Chen:** Resources. **Chin-Pao Huang:** Conceptualization, Writing - review & editing, Project administration, Supervision, Funding acquisition.

Declaration of Competing Interest

The authors reported no declarations of interest.

Acknowledgement

The materials presented in this paper were based upon work partially supported by National Science Foundation, Grant No. 0965984 under the Environmental Engineering Program, Division of Chemical, Bioengineering, Environmental, and Transport Systems. J. F. Su also acknowledges the support by the Ministry of Science and Technology, Taiwan (109-2222-E-032 -001) and 109-2221-E-032-040-MY2.

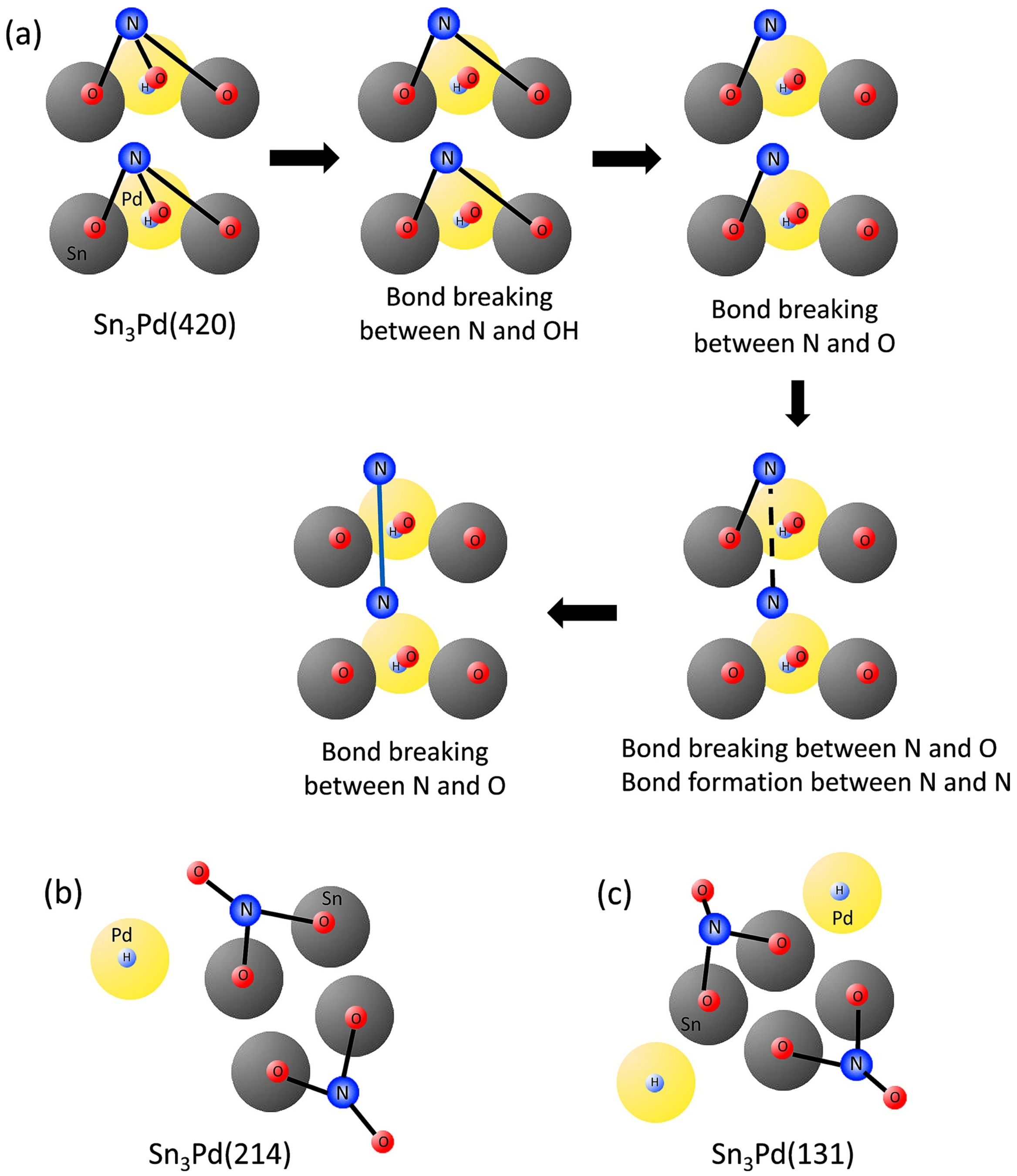

Fig. 10. Illustration of predicted nitrate reduction mechanism on SS/Sn-Pd electrodes with (a) $Sn_3Pd(420)$, (b) $Sn_3Pd(214)$, and (c) $Sn_3Pd(131)$ planes. The main feature of the proposed reaction mechanism in (a) are: (1) adsorption of nitrate onto an empty Sn site via their oxygen atom; (2) the adsorption of hydrogen on the empty Pd site; (3) the bond breaking reaction between N and OH; (4) the bond breaking reaction between N and O; (5) the bond formation reaction between adjacent two N atoms; (6) the final bond breaking reaction between N and O, leading to the formation of N_2. In (b) and (c), the bond breaking reaction between N and OH is more difficult in $Sn_3Pd(214)$ and $Sn_3Pd(131)$ likely due to the steric restrictions.

Appendix A. Supplementary data

Supplementary material related to this article can be found, in the online version, at doi:https://doi.org/10.1016/j.apcata.2020.117809.

References

[1] B.-U. Bae, Y.-H. Jung, W.-W. Han, H.-S. Shin, Water Res. 36 (2002) 3330–3340, https://doi.org/10.1016/S0043-1354(02)00012-X.

[2] J.J. Schoeman, A. Steyn, Desalination 155 (2003) 15–26, https://doi.org/10.1016/S0011-9164(03)00235-2.

[3] L.J. Banasiak, A.I. Schäfer, J. Memb. Sci. 334 (2009) 101–109, https://doi.org/10.1016/j.memsci.2009.02.020.

[4] K. Anoop, V. T, J. Environ. Eng. New York (New York) 123 (1997) 371–380, https://doi.org/10.1061/(ASCE)0733-9372(1997)123:4(371).

[5] G.K. Luk, W.C. Au-Yeung, Adv. Environ. Res. 6 (2002) 441–453, https://doi.org/10.1016/S1093-0191(01)00072-7.

[6] C. Della Rocca, V. Belgiorno, S. Meriç, Desalination 204 (2007) 46–62, https://doi.org/10.1016/j.desal.2006.04.023.

[7] X. Fan, X. Guan, J. Ma, H. Ai, J. Environ. Sci. China (China) 21 (2009) 1028–1035, https://doi.org/10.1016/S1001-0742(08)62378-5.

[8] C.P. Huang, H.W. Wang, P.C. Chiu, Water Res. 32 (1998) 2257–2264, https://doi.org/10.1016/S0043-1354(97)00464-8.

[9] J.M. Rodríguez-Maroto, F. García-Herruzo, A. García-Rubio, C. Gómez-Lahoz, C. Vereda-Alonso, Chemosphere 74 (2009) 804–809, https://doi.org/10.1016/j.chemosphere.2008.10.020.

[10] K.N. Heck, S. Garcia-Segura, P. Westerhoff, M.S. Wong, Acc. Chem. Res. 52 (2019)

906–915, https://doi.org/10.1021/acs.accounts.8b00642.

[11] D. He, Y. Li, H. Ooka, Y.K. Go, F. Jin, S.H. Kim, R. Nakamura, J. Am. Chem. Soc. 140 (2018) 2012–2015, https://doi.org/10.1021/jacs.7b12774.

[12] B. Shen, Z. Liu, H. Xu, F. Wang, Fuel 235 (2019) 878–885, https://doi.org/10.1016/J.FUEL.2018.08.082.

[13] Y.A. Shao, Y.T. Chen, P.Y. Chen, Electrochim. Acta 313 (2019) 488–496, https://doi.org/10.1016/j.electacta.2019.05.057.

[14] S. Garcia-Segura, M. Lanzarini-Lopes, K. Hristovski, P. Westerhoff, Appl. Catal. B Environ. 236 (2018) 546–568, https://doi.org/10.1016/j.apcatb.2018.05.041.

[15] J. Gao, B. Jiang, C. Ni, Y. Qi, Y. Zhang, N. Oturan, M.A. Oturan, Appl. Catal. B Environ. 254 (2019) 391–402, https://doi.org/10.1016/j.apcatb.2019.05.016.

[16] N. Aouina, H. Cachet, C. Debiemme-chouvy, T.T.M. Tran, Electrochim. Acta 55 (2010) 7341–7345, https://doi.org/10.1016/j.electacta.2010.07.032.

[17] O.A. Petrii, T.Y. Safonova, J. Electroanal. Chem. Lausanne (Lausanne) 331 (1992) 897–912, https://doi.org/10.1016/0022-0728(92)85013-S.

[18] G.E. Dima, A.C.A. de Vooys, M.T.M. Koper, J. Electroanal. Chem. Lausanne (Lausanne) 554–555 (2003) 15–23, https://doi.org/10.1016/S0022-0728(02)01443-2.

[19] K. Bouzek, M. Paidar, A. Sadílková, H. Bergmann, J. Appl. Electrochem. 31 (2001) 1185–1193, https://doi.org/10.1023/A:1012755222981.

[20] S. Cattarin, J. Appl. Electrochem. 22 (1992) 1077–1081, https://doi.org/10.1007/BF01029588.

[21] P.M. Tucker, M.J. Waite, B.E. Hayden, J. Appl. Electrochem. 34 (2004) 781–796, https://doi.org/10.1023/B:JACH.0000035607.19248.b6.

[22] I. Katsounaros, D. Ipsakis, C. Polatides, G. Kyriacou, Electrochim. Acta 52 (2006) 1329–1338, https://doi.org/10.1016/j.electacta.2006.07.034.

[23] J.D. Genders, D. Hartsough, D.T. Hobbs, J. Appl. Electrochem. 26 (1996) 1–9, https://doi.org/10.1007/BF00248182.

[24] T.Y. Safonova, O.A. Petrii, J. Electroanal. Chem. Lausanne (Lausanne) 448 (1998) 211–216, https://doi.org/10.1016/S0022-0728(97)00110-1.

[25] C. Polatides, G. Kyriacou, J. Appl. Electrochem. 35 (2005) 421–427, https://doi.org/10.1007/s10800-004-8349-z.

[26] Z. Mácová, K. Bouzek, J. Appl. Electrochem. 35 (2005) 1203–1211, https://doi.org/10.1007/s10800-005-9028-4.

[27] Y. Zhang, Y. Zhao, Z. Chen, L. Wang, L. Zhou, P. Wu, F. Wang, P. Ou, J. Electrochem. Soc. 165 (2018) E420–E428, https://doi.org/10.1149/2.0081810jes.

[28] Y. Zhang, Y. Zhao, Z. Chen, L. Wang, P. Wu, F. Wang, Electrochim. Acta 291 (2018) 151–160, https://doi.org/10.1016/j.electacta.2018.08.154.

[29] L. Lemaignen, C. Tong, V. Begon, R. Burch, D. Chadwick, Catal. Today 75 (2002) 43–48, https://doi.org/10.1016/S0920-5861(02)00042-1.

[30] A.C.A. de Vooys, R.A. van Santen, J.A.R. van Veen, J. Mol. Catal. A Chem. 154 (2000) 203–215, https://doi.org/10.1016/S1381-1169(99)00375-1.

[31] D. Reyter, D. Bélanger, L. Roué, J. Phys. Chem. C. 113 (2009) 290–297, https://doi.org/10.1021/jp805484t.

[32] J.F. Su, I. Ruzybayev, I. Shah, C.P. Huang, Appl. Catal. B Environ. 180 (2016) 199–209, https://doi.org/10.1016/j.apcatb.2015.06.028.

[33] K. Shimazu, R. Goto, K. Tada, Chem. Lett. 31 (2002) 204–205, https://doi.org/10.1246/cl.2002.204.

[34] J.F. Su, W.F. Kuan, H. Liu, C.P. Huang, Appl. Catal. B Environ. 257 (2019) 117909, https://doi.org/10.1016/j.apcatb.2019.117909.

[35] A.S. Bandarenka, M.T.M. Koper, J. Catal. 308 (2013) 11–24, https://doi.org/10.1016/j.jcat.2013.05.006.

[36] D. Reyter, D. Bélanger, L. Roué, Water Res. 44 (2010) 1918–1926, https://doi.org/10.1016/j.watres.2009.11.037.

[37] D. Reyter, D. Bélanger, L. Roué, J. Hazard. Mater. 192 (2011) 507–513, https://doi.org/10.1016/j.jhazmat.2011.05.054.

[38] L. Li, Y. Yun, Y. Zhang, Y. Huang, Z. Xu, J. Alloys. Compd. 766 (2018) 157–160, https://doi.org/10.1016/j.jallcom.2018.07.004.

[39] T. Chen, H. Li, H. Ma, M.T.M. Koper, Langmuir 31 (2015) 3277–3281, https://doi.org/10.1021/acs.langmuir.5b00283.

[40] M. Duca, M.O. Cucarella, P. Rodriguez, M.T.M. Koper, J. Am. Chem. Soc. 132 (2010) 18042–18044, https://doi.org/10.1021/ja1092503.

[41] M. Duca, M.C. Figueiredo, V. Climent, P. Rodriguez, J.M. Feliu, M.T.M. Koper, J. Am. Chem. Soc. 133 (2011) 10928–10939, https://doi.org/10.1021/ja203234v.

[42] D.F. van der Vliet, M.T.M. Koper, Surf. Sci. 604 (2010) 1912–1918, https://doi.org/10.1016/j.susc.2010.07.027.

[43] I. Katsounaros, M.C. Figueiredo, X. Chen, F. Calle-Vallejo, M.T.M. Koper, Electrochim. Acta 271 (2018) 77–83, https://doi.org/10.1016/j.electacta.2018.03.126.

[44] H. Li, F. Calle-Vallejo, M.J. Kolb, Y. Kwon, Y. Li, M.T.M. Koper, J. Am. Chem. Soc. 135 (2013) 14329–14338, https://doi.org/10.1021/ja406655q.

[45] M. Kato, M. Okui, S. Taguchi, I. Yagi, J. Electroanal. Chem. Lausanne (Lausanne) 800 (2017) 46–53, https://doi.org/10.1016/j.jelechem.2017.01.020.

[46] F. Epron, F. Gauthard, C. Pinéda, J. Barbier, J. Catal. 198 (2001) 309–318, https://doi.org/10.1006/jcat.2000.3138.

[47] F. Epron, F. Gauthard, J. Barbier, Appl. Catal. A Gen. 237 (2002) 253–261, https://doi.org/10.1016/S0926-860X(02)00331-9.

[48] R. Zhang, D. Shuai, K.A. Guy, J.R. Shapley, T.J. Strathmann, C.J. Werth, ChemCatChem. 5 (2013) 313–321, https://doi.org/10.1002/cctc.201200457.

[49] J. Martínez, A. Ortiz, I. Ortiz, Appl. Catal. B Environ. 207 (2017) 42–59, https://doi.org/10.1016/j.apcatb.2017.02.016.

[50] U. Prüsse, K.-D. Vorlop, J. Mol. Catal. A Chem. 173 (2001) 313–328, https://doi.org/10.1016/S1381-1169(01)00156-X.

[51] K. Shimazu, R. Goto, S. Piao, R. Kayama, K. Nakata, Y. Yoshinaga, J. Electroanal. Chem. Lausanne (Lausanne) 601 (2007) 161–168, https://doi.org/10.1016/j.jelechem.2006.11.005.

[52] M. Motahar Hossain, K. Nakata, T. Kawaguchi, K. Shimazu, J. Electroanal. Chem. Lausanne (Lausanne) 707 (2013) 59–65, https://doi.org/10.1016/j.jelechem.2013.08.015.

[53] S. Sadjadi, M. Atai, Appl. Clay Sci. 153 (2018) 78–89, https://doi.org/10.1016/j.clay.2017.12.013.

[54] S. Navaladian, B. Viswanathan, T.K. Varadarajan, R.P. Viswanath, Nanoscale Res. Lett. 4 (2008) 181, https://doi.org/10.1007/s11671-008-9223-4.

[55] S. Hamid, S. Bae, W. Lee, Chem. Eng. J. 348 (2018) 877–887, https://doi.org/10.1016/j.cej.2018.05.016.

[56] A. Banotra, N. Padha, J. Korean Inst. Electr. Electron. Mater. Eng. 48 (2019) 304–311, https://doi.org/10.1007/s11664-018-6710-y.

[57] H. Chen, Q. Ye, X. He, J. Ding, Y. Zhang, J. Han, J. Liu, C. Liao, J. Mei, W. Lau, Green Chem. 16 (2014) 3841–3845, https://doi.org/10.1039/C4GC00142G.

[58] L. Zhang, A.A.S. Gonçalves, M. Jaroniec, RSC Adv. 10 (2020) 5585–5589, https://doi.org/10.1039/D0RA00769B.

[59] Y. Yoshinaga, T. Akita, I. Mikami, T. Okuhara, J. Catal. 207 (2002) 37–45, https://doi.org/10.1006/jcat.2002.3529.

[60] Y.J. Shih, Z.L. Wu, Y.H. Huang, C.P. Huang, Chem. Eng. J. 383 (2020) 123157, https://doi.org/10.1016/j.cej.2019.123157.

[61] H. Sitepu, B.H. O'Connor, D. Li, J. Appl. Crystallogr. 38 (2005) 158–167, https://doi.org/10.1107/S0021889804031231.

[62] S. Hamid, M.A. Kumar, W. Lee, Appl. Catal. B Environ. 187 (2016) 37–46, https://doi.org/10.1016/j.apcatb.2016.01.035.

[63] J. Sá, D. Gasparovicova, K. Hayek, E. Halwax, J.A. Anderson, H. Vinek, Catal. Letters 105 (2005) 209–217, https://doi.org/10.1007/s10562-005-8692-7.

[64] M.R. Shoar Abouzari, F. Berkemeier, G. Schmitz, D. Wilmer, Solid State Ion. 180 (2009) 922–927, https://doi.org/10.1016/j.ssi.2009.04.002.

[65] Y. Wang, J. Qu, R. Wu, P. Lei, Water Res. 40 (2006) 1224–1232, https://doi.org/10.1016/j.watres.2006.01.017.

[66] H. Li, Y. Li, M.T.M. Koper, F. Calle-Vallejo, J. Am. Chem. Soc. 136 (2014) 15694–15701, https://doi.org/10.1021/ja508649p.

[67] R.R. Adić, N.M. Marković, V.B. Vešović, J. Electroanal. Chem. Interfacial Electrochem. 165 (1984) 105–120, https://doi.org/10.1016/S0022-0728(84)80090-X.

[68] R.R. Adžić, S. Strbac, N. Anastasijević, Mater. Chem. Phys. 22 (1989) 349–375, https://doi.org/10.1016/0254-0584(89)90005-9.

[69] Y. Hori, I. Takahashi, O. Koga, N. Hoshi, J. Phys. Chem. B 106 (2002) 15–17, https://doi.org/10.1021/jp013478d.

[70] F.J. Vidal-Iglesias, N. García-Aráez, V. Montiel, J.M. Feliu, A. Aldaz, Electrochem. commun. 5 (2003) 22–26, https://doi.org/10.1016/S1388-2481(02)00521-0.

[71] F.J. Vidal-Iglesias, J. Solla-Gullón, V. Montiel, J.M. Feliu, A. Aldaz, J. Phys. Chem. B 109 (2005) 12914–12919, https://doi.org/10.1021/jp051269d.